frontiers | Frontiers in Energy Research

TYPE Original Research
PUBLISHED 04 January 2024
DOI 10.3389/fenrg.2023.1321853

OPEN ACCESS

EDITED BY
Peng Tan,
CNPC Engineering Technology R&D Company Limited, China

REVIEWED BY
Chunxiao Li,
China University of Geosciences Wuhan, China
Yong Zheng,
Xi'an Shiyou University, China
Song Deng,
Changzhou University, China
Zizhen Wang,
China University of Petroleum (East China), China
Rui Liu,
Southwest Petroleum University, China
Chao Liu,
Aramco Services Company, United States

*CORRESPONDENCE
Mao Sheng,
shengmao@cup.edu.cn

RECEIVED 15 October 2023
ACCEPTED 13 December 2023
PUBLISHED 04 January 2024

CITATION
Cheng S, Sheng M and Deng C (2024), Identification of different lithofacies laminations in oil shale and their mechanical properties.
Front. Energy Res. 11:1321853.
doi: 10.3389/fenrg.2023.1321853

Identification of different lithofacies laminations in oil shale and their mechanical properties

Shizhong Cheng, Mao Sheng* and Chao Deng

National Key Laboratory of Petroleum Resources and Engineering, China University of Petroleum (Beijing), Beijing, China

Lamination can greatly enhance the anisotropy and heterogeneity of shale and plays a significant role in influencing hydraulic fracturing. The structure and mechanical difference of different lithofacies lamination are the basis to reveal the fracture propagation mechanism. In this paper, research focused on three continental oil shale with different lithofacies in Qikou sag, Bohai Bay basin, including Quartz-Feldspar dominated shale, Carbonate dominated shale and mixed-mineral shale. Scanning electron microscopy and mineral analysis are used to identify quartz-feldspar lamination and mixture lamination in Quartz-Feldspar dominated shales, as well as carbonate lamination and mixture lamination in Carbonate dominated shales. The distinct laminations with different characteristics were precisely located using FIB, which served as the guiding tool for the indentation experiment. The micromechanical properties of laminations with different lithofacies in oil shale samples are examined using the nanoindentation technique, highlighting their distinct differences. The findings demonstrate that the micromechanical properties of quartz-feldspar lamination in Quartz-Feldspar dominated shales exhibit superior strength, while the mechanical difference between laminations in Quartz-Feldspar dominated shales are significantly larger. The quartz-feldspar lamination exhibits the highest resistance when subjected to indentation force. The mechanical properties of mixture lamination in Quartz-Feldspar dominated shales and Carbonate dominated shales are comparable due to their similar mineral composition. Moreover, in conjunction with macroscopic rock mechanics experiments, it has been verified that the lamination structure facilitates the initiation and propagation of macroscopic fractures under stress loading.

KEYWORDS

oil shale, micromechanics, lamination, lithofacies, nanoindentation

1 Introduction

With the extensive research on shale gas theory and the rapid advancements in exploration and development, laminated oil shale has garnered significant attention and recognition in recent years (Zhijun et al., 2021). Since the weak strength is distributed along the bedding planes, the direction of the bedding plane determines the failure mode. The special failure mode of laminated shale is different from that of isotropic formation, which is

Abbreviations: CL, Carbonate (calcite, dolomite) lamination; CS, Carbonate dominated shale; ML, Mixture lamination; MS, Mixed mineral shale; QFS, Quartz-Feldspar dominated shale; QFL, Quartz-Feldspar lamination.

controlled by bedding inclination and *in-situ* stress (Chenevert and Gatlin, 1965; Niandou et al., 1997). Due to its exceptional reservoir physical properties, laminated oil shale reservoir is more amenable to reformation, resulting in high production. Also, laminations have great influence on the mechanical properties of oil shale. The utilization of high-resolution testing methods to examine the mechanical properties of laminations in shale, thereby elucidating the fracture initiation mechanism, holds immense significance.

It has been proved that the lamination can significantly improve the anisotropy of shale (Vernik and Nur, 1992; Sayers, 2013; Li et al., 2017; Jin et al., 2018; Vernik and Nur, 1992) observed laminated black shale from Bakken formation. The scale of lamination is in the range of 0.2–3 mm through thin sections and up to 10–15 μm through back-scatter SEM (Scanning electron microscope). The gas-bearing shales of the Longmaxi Formation were analyzed by SHI et al. (2020) using thin section imaging and microscope observation, revealing two distinct lamination structures: muddy lamination with an average thickness of 76.54 μm and silty lamination with an average thickness of 54.14 μm (Mokhtari et al., 2014). observed calcite-filled discontinuities in Eagle Ford shale through thin-section and verified that tensile strength along lamination is always lower than that across lamination (Li et al., 2017). proposed a model to simulate the anisotropic mechanical behavior of shale with considering direction of laminations and elucidated directional dependence of tensile and compressive strengths. Subsequently, abundant research began to study the effect of lamination (Liu et al., 2020; Zhang et al., 2022) or heterogeneity (Huang et al., 2019; Huang et al., 2023) on fracture propagation through numerical simulation, macroscopic mechanics (Huang et al., 2020; Yang et al., 2021) and fracturing experiments (Lei et al., 2021; Yang et al., 2021) developed a novel constitutive model to investigate fracture evolution behavior in layered rock with considering the mechanical behavior of soft layers and hard layers as well as layer interfaces. Results demonstrated that bedding inclination angle greatly influenced finale fracture pattern of the layered rock (Tan et al., 2017; Tan et al., 2023). focused on initiation and vertical propagation of fractures in laminated shale formations through large-scale tri-axial experiments and concluded that lamination significantly influences the propagation of fracture height combined with numerical model (Tan et al., 2021).

Although the lamination or bedding of shale is widely acknowledged as a crucial geometrical factor that significantly influences the mechanical anisotropy and fracture propagation, there remains limited research on the mechanical characterization of lamination at the microscopic level. Nanoindentation technique has been successfully applied in the measurement of shale micromechanics (Li et al., 2019; Sheng et al., 2022; Ulm and Abousleiman, 2006; Ulm et al., 2007) developed grid-indentation and combined deconvolution approach to conduct statistical analysis on heterogeneous and anisotropic properties of shale (Cheng et al., 2021). have preliminarily identified the lamination in Longmaxi shale and carried out micromechanical tests to compare the micromechanical differences of lamination with different particle sizes. Therefore, further research on more detailed lamination characteristics, micromechanics and fracture mechanics is needed.

In this paper, three laminations with different lithofacies of oil shale in the Third Member of Shahejie Formation in Qikou sag, Bohai Bay basin were identified through SEM and mineral analysis. The distinct laminations with different characteristics were precisely identified using FIB (Focused ion beam), which served as the guiding tool for the indentation experiment. The nanoindentation approach was utilized to quantify the micro mechanical properties of three different laminations. The paper explores the mechanical variations among laminae in different lithofacies and demonstrates that the mechanical properties of laminae in Quartz-Feldspar dominated shales exhibit significant disparities, thereby facilitating interlamina fractures formation. Moreover, in conjunction with macroscopic rock mechanics experiments, it has been verified that the lamination structure facilitates the initiation and propagation of macroscopic fractures under stress loading.

2 Materials and methods

2.1 Material and specimen preparation

Three distinct shale samples were collected from the downhole cores at Shahejie Formation in Qikou sag, Bohai Bay basin. Qikou sag is located in the hinterland of Huanghua Depression. The effective exploration area of the paleogene in Qikou Sag is 5.28 × 103 km^2, and the main source rocks are from Sha-3 Member and Sha-1 Member (Xiugang et al., 2023). The samples are from Sha-3 Member and there measured depths are 4076, 4051 and 4000 m, respectively.

The mineral composition of three core samples was determined through XRD analysis according to the Standard SY/T 5163-2010, and the results are presented in Table 1. According to the chemical composition of the mineral, the mineral composition in the sample is divided into three types: Clay minerals, Quartz-Feldspar dominated minerals and Carbonate dominated minerals (Maowen et al., 2022). Other minerals were also quantitatively analyzed according to the standards. The lithofacies division is carried out based on the whole rock mineral composition, as shown in Figure 1. The lithofacies of three downhole samples are Quartz-Feldspar dominated shale (QFS), Mixed mineral shale (MS) and Carbonate dominated shale (CS).

The cubical specimen (10 mm length × 5 mm width × 2 mm height) were cut from the shale samples. Sample surfaces were firstly polished by using sanding paper meshing from 180# to 4000#. First mechanical polish is to achieve surface roughness of less than 0.5 micron. High energy argon ion beam was used in next polish step and continuously conducted for 2 h to achieve surface roughness less than 100 nm. The target surface for micromechanical testing was oriented perpendicular to the shale bedding planes, as depicted in Figure 1, allowing for the visualization of the laminated sedimentary structure.

2.2 Experimental methodology

SEM, EDS (Energy Dispersive Spectrometer) and FIB were conducted firstly to identify and locate different lithofacies laminations. Then, micromechanical properties of lamination could be quantified through nanoindentation tests. Uniaxial compression tests were carried out to verify the influence of laminations on macro fractures. The micromechanical and macroscopic mechanical samples were obtained from the downhole core of the same geological layer shown in Figure 1.

TABLE 1 Mineral composition of three distinct core samples.

Sample	Depth, m	Composition, wt%							Lithofacies
		Quartz	Feldspar	Calcite	Dolomite	Clay	Pyrite	Others	
1	4076.83	36.0	14.8	9.7	8.9	27.5	1.9	1.2	Quartz-Feldspar dominated shale (QFS)
2	4051.44	23.5	6.6	20.2	7.9	36.1	3.1	2.6	Mixed mineral shale (MS)
3	4000.7	13.3	3.4	24.6	28.7	26.0	2.6	1.4	Carbonate dominated shale (CS)

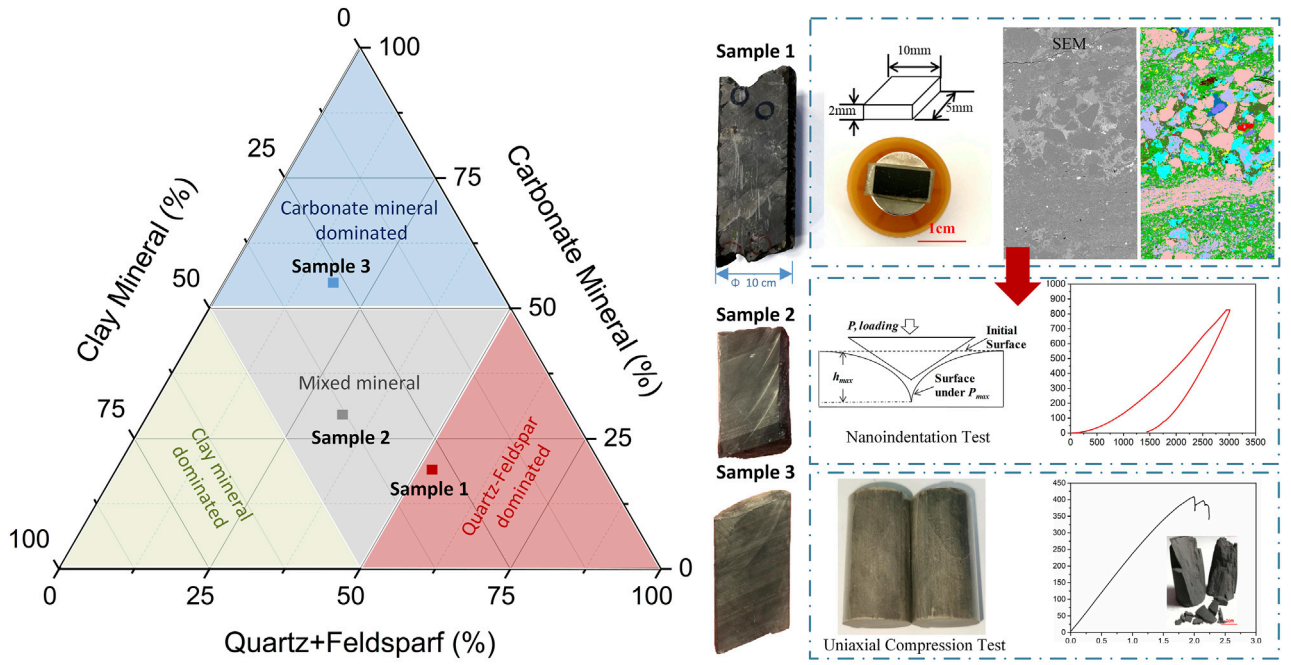

FIGURE 1
Lithofacies classification and experimental design scheme.

2.2.1 SEM

Different mineral laminations were observed firstly through SEM (ZEISS Merlin, ZEISS, Germany) and analyzed through EDS in three different lithofacies samples. Subsequently, FIB was employed to precisely locate distinct mineral laminations by utilizing a high current ion beam, ensuring the accurate identification of lamination features during optical microscope navigation in the nanoindentation device. Through micromechanical testing, the disparities in micromechanical properties among different lithologic laminations are ultimately elucidated. Then, FIB was performed to mark the beginning and end of the target lamination to ensure the correct position and angle of the lamination, as shown in Figure 2.

2.2.2 Nanoindentation

Nanoindentation (G200, Keysight, America) was conducted with continuous stiffness measurement (CSM) mode, which enables continuous measurement of mechanical properties over the indentation depth. The target lamination can be accurately located by recognizing FIB markers in optical microscope navigation in nanoindentation equipment. Furthermore, 1 × 10 points are arranged in each lamination, the point spacing is 100 microns, and the ultimate indent depth is 3,000 nm which could eliminate interaction between individual points and facilitate the measurement of minerals and mineral phases at multiple scales (Ulm and Abousleiman, 2006). In CSM mode, a harmonic oscillator is employed for the indenter, which can be considered as a cyclic loading process depicted in Figure 2D. For each load cycle, The elastic modulus and hardness at that depth are determined using the same computational approach as described below (Phani et al., 2020). The selection of a Berkovich diamond indenter in nanoindentation was based on its high spring constant range and ability for the measurement of composite materials with a wide range of elastic modulus.

The Young's modulus and hardness were determined by employing the following Eqs. (1–4) based on the load-displacement curve (Oliver and Pharr, 1992; Sheng et al., 2022):

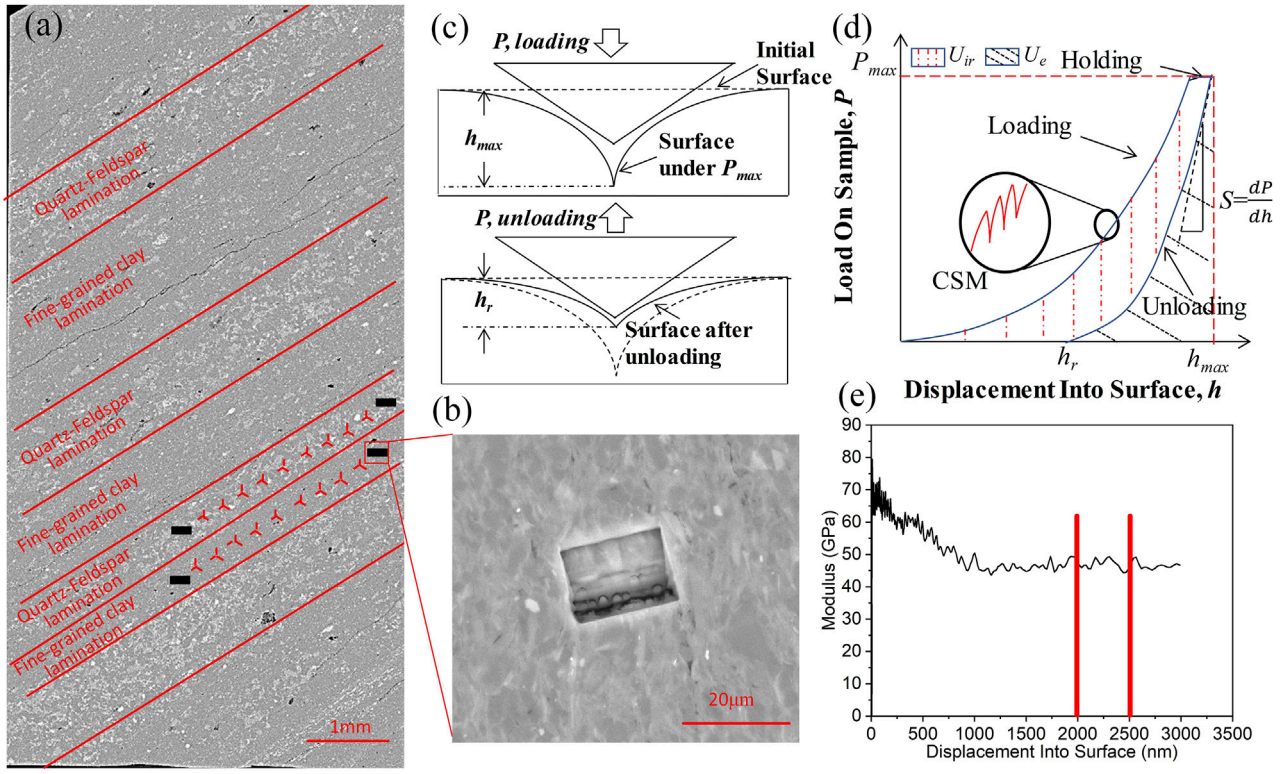

FIGURE 2
Nanoindentation schematic: **(A)** Grid indentations on laminations; **(B)** FIB marker; **(C)** Indentation scheme; **(D)** Nanoindentation load on sample-displacement into surface curve and continuous stiffness measurement (CSM) diagram; **(E)** CSM result example: Change of elastic modulus with indentation depth.

$$\frac{1}{E_{reduced}} = \frac{\left(1-\nu_{sample}\right)^2}{E_{sample}} + \frac{\left(1-\nu_{tip}\right)^2}{E_{tip}} \quad (1)$$

$$E_r = \frac{\sqrt{\pi}}{2}\frac{S}{\sqrt{A_c}} \quad (2)$$

$$H = \frac{P_{\max}}{A_c} \quad (3)$$

$$S = \frac{dP}{dh}\Big|_{h=h_{\max}} \quad (4)$$

Where, E_{reduced} is the reduced modulus; ν and E are Poisson's ratio and Young's modulus; $P_{\max}$ is the maximum load. S is the stiffness as shown in Figure 2D. A_c is the projected contact area. For Berkovich indenters, $A_c = 24.56h_c^2 + Ch_c$. C is a constant obtained in the calibration.

According to the indentation energy analysis method theory (Cheng et al., 2002; Liu et al., 2016; Zeng et al., 2017), the fracture toughness of indentation point could be calculated through Eqs (5–9):

$$U_{ir} = U_t - U_e \quad (5)$$

$$U_f = U_{ir} - U_{pp} \quad (6)$$

$$\frac{U_{pp}}{U_t} = 1 - \left[\frac{1-3\left(\frac{h_f}{h_{\max}}\right)^2 + 2\left(\frac{h_f}{h_{\max}}\right)^3}{1-\left(\frac{h_f}{h_{\max}}\right)^2}\right] \quad (7)$$

Where, U_{ir} is the irreversible energy, U_t is the total energy, U_e is the recoverable elastic energy, U_f is the fracture energy, and U_{pp} is the pure plastic energy. The relationship between critical energy release rate G_c and fracture energy U_f is as follows:

$$G_c = \frac{dU_f}{dA} = \frac{U_f}{A_{\max}} \quad (8)$$

The fracture toughness can be determined through the subsequent formula.

$$K_{ic} = \sqrt{G_c E_r} \quad (9)$$

2.2.3 Uniaxial compression test

The traditional uniaxial compression tests were conducted on the samples cut from the same part of the downhole core. The displacement-control mode was selected in the experiment. The loading rate was set at 0.04 mm/min, and a dual-channel acoustic emission system was incorporated during the experimental procedure. Stress-strain curves and AE counts were recorded. The sample's failure pattern was exhibited through photography.

3 Results and discussions

3.1 Identification of different lithological laminations

The lamination structure in different lithofacies shales was identified by SEM and mineral analysis (Vernik and Nur, 1992). observed laminated black shale from Bakken formation. The scale of lamination is in the range of 0.2–3 mm. And (SHI et al., 2020), using

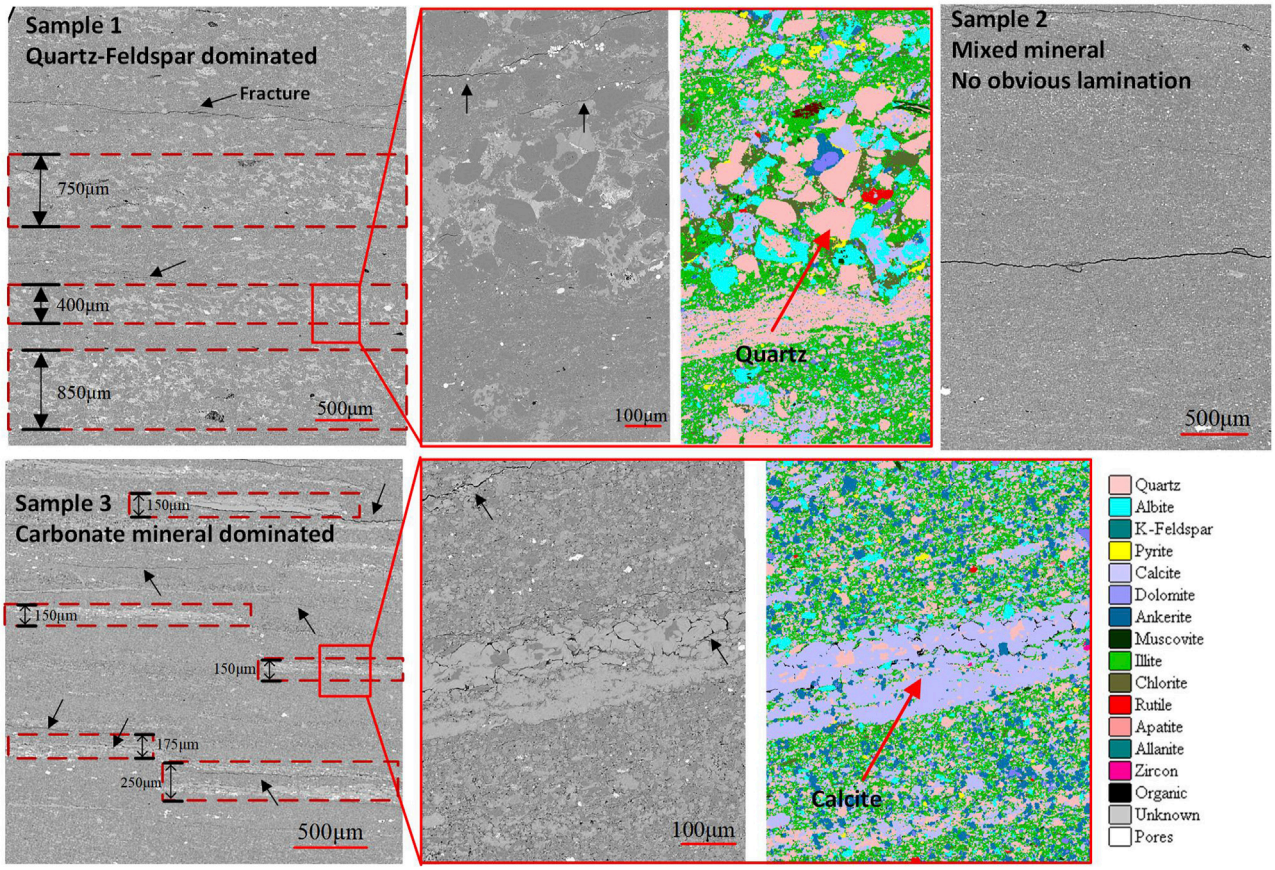

FIGURE 3
Typical laminations in different lithofacies samples. The developed laminations are enclosed by red rectangular. The black arrow points to the fractures.

TABLE 2 Shale lithofacies and their corresponding lamination component.

Shale lithofacies	Lamination component
QFS (Quartz-Feldspar dominated shale)	QFL (Quartz-Feldspar lamination)
	ML (Mixture lamination)
CS (Carbonate dominated shale)	CL (Carbonate lamination)
	ML (Mixture lamination)
MS (Mixed mineral shale)	No obvious laminations

thin section imaging and microscope observation, revealing two distinct lamination structures: muddy lamination with an average thickness of 76.54 μm and silty lamination with an average thickness of 54.14 μm. Previous studies identified shale bedding layers with various grain sizes (Cheng et al., 2021). However, it does not provide a detailed analysis of the specific components. In this study, the qualitative interpretation and quantitative analysis of different lithofacies laminations were carried out. Figure 3 shows the typical laminations in different lithofacies samples. The lamination characteristics observed in three lithofacies shale are shown in Table 2. In QFS, as shown in Sample 1, the lamination is characterized by alternating deposition of QFL and ML. QFL is composed of large grains (grain size>50 μm) of quartz and feldspar minerals, while ML is mainly composed of fine-grained clay mineral particles. In CS, as shown in Sample 3, the main laminations are CL and ML. However, in MS, lamination is not well developed, as shown in Sample 2. The mineral particles in the MS exhibit a more homogeneous dispersion pattern. The thickness of QFL in Sample 1 is relatively substantial, exceeding 400 μm on average. The observed carbonate laminations are consistently smaller than 300 μm.

Furthermore, the development of fractures can be discerned through the morphology observed in SEM. In MS, there are several primary fractures with relatively uncomplicated geometries. However, in QFS and CS, the development of lamination can induce a greater number of micro-fractures along the edges of mineral grains and enhance fracture complexity. These fractures predominantly occur at the junctions between lamination layers, indicating that these interfaces are inherently weak and susceptible to opening or communicate during fracturing.

3.2 Micromechanical differences of different lithological laminations

According to the different lithofacies lamination characteristics identified in Section 3.1, micron indentation experiments are carried

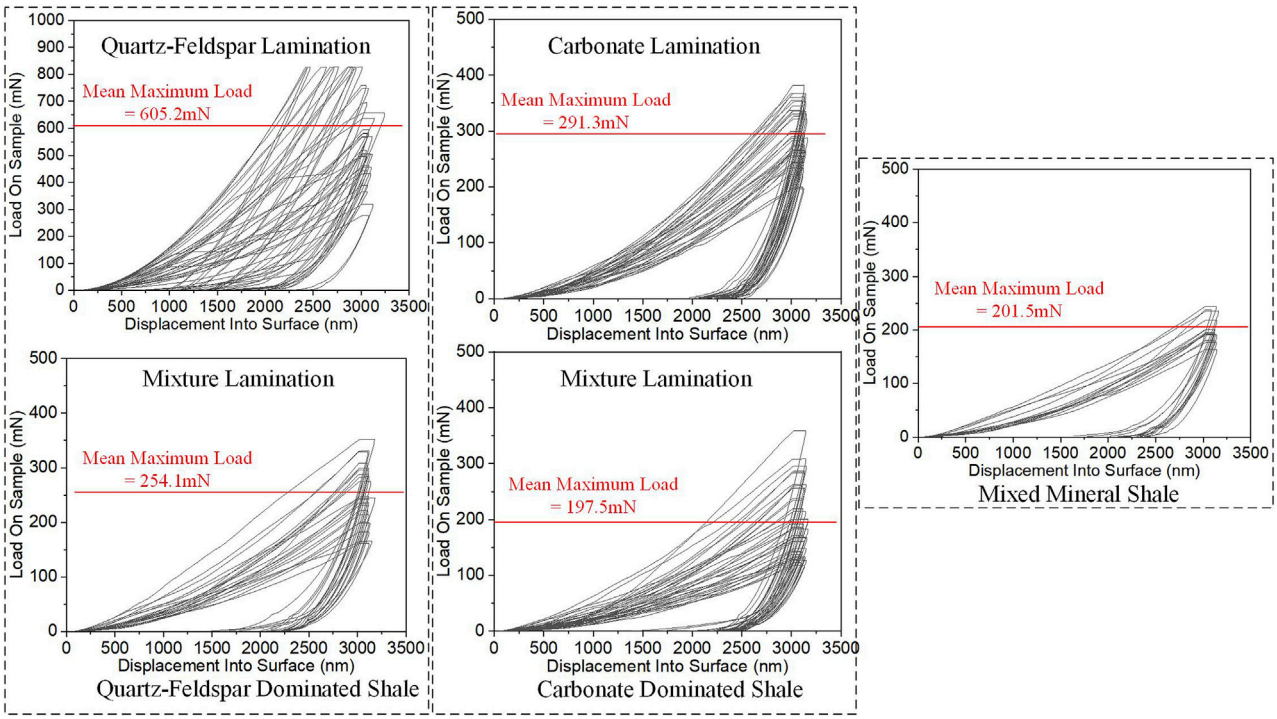

FIGURE 4
Displacement into Surface vs. Load on Sample curves at each indentation point.

out. In MS, no obvious lamination structure is observed, the mineral particles are uniformly distributed so that the micro indentation experiments were conducted randomly on the sample surface to avoid local effects. The load on sample vs. displacement into surface curves at each indentation point were shown in Figure 4. The mean maximum load in QFL was the highest, indicating that indenting QFL posed the greatest difficulty. This is due to the development of feldspar and quartz minerals in the QFL, which show a strong hardness. The mean maximum load in ML in QFS and CS are similar with that in MS because of the similar clay mineral composite. In particular, within the QFL, multiple curves demonstrate that when the displacement falls short of reaching the predetermined indentation depth of 3,000 nm, the load attains its maximum value. This further substantiates the high strength exhibited by QFL.

The characteristics of elastic modulus and hardness data of different lithological laminations were analyzed by interquartile range and variance, as shown in Figure 5. The elastic modulus and hardness of the quartz-feldspar lamination in QFS are the highest among the different lithofacies laminations. In QFS and CS, micro indentation experiments were conducted inside laminations. In QFS, the elastic modulus of QFL is 55% higher than that of ML, and the hardness is 232% higher. In CS, the elastic modulus and hardness of CL are 33% higher and 53% higher than that of ML. The elastic modulus and hardness of ML in QFS and CS are comparable to those observed in MS, as the composition of ML in both types of shales closely resembles that of MS, characterized by fine clay particles.

The fracture toughness of the indentation point was calculated from the displacement-load curves. The results unequivocally demonstrate the robust fracture toughness of QFL in Figure 6. The results show that the difference of fracture mechanics between the two types of lamination in QFS is the largest, while the difference of fracture mechanics between the two types of CS is small.

3.3 Effect of lamination structure on the formation and propagation of macroscopic cracks

Previous studies have confirmed that in the macroscopic rock mechanics and Brazilian tests considering the direction of bedding, cracks are prone to cracking along the bedding plains or laminations (Zhu et al., 2021). The lamination structure and mechanical difference among laminations facilitate the initiation of microcracks, which are prone to propagate into macro-cracks under loading conditions. Simulations have also verified that bedding or lamination structures greatly influence the mechanical properties and failure mode of shale rocks (Li et al., 2017). True tri-axial hydraulic fracturing experiments have been conducted to elucidated hydraulic fracture initiation and propagation was influenced by bedding plane (Tan et al., 2017). In this study, we have elucidated the distinct lithological lamination structure and micromechanical variations of laminations in shale, which serve as the microphysical and mechanical foundation for determining the initiation and propagation of macroscopic fractures.

Cylindrical samples were drilled from downhole core samples to carry out uniaxial compression experiments. Figure 7 illustrates the observed sample failure characteristics, stress-strain curve, and acoustic emission counting results from the experiment. Acoustic

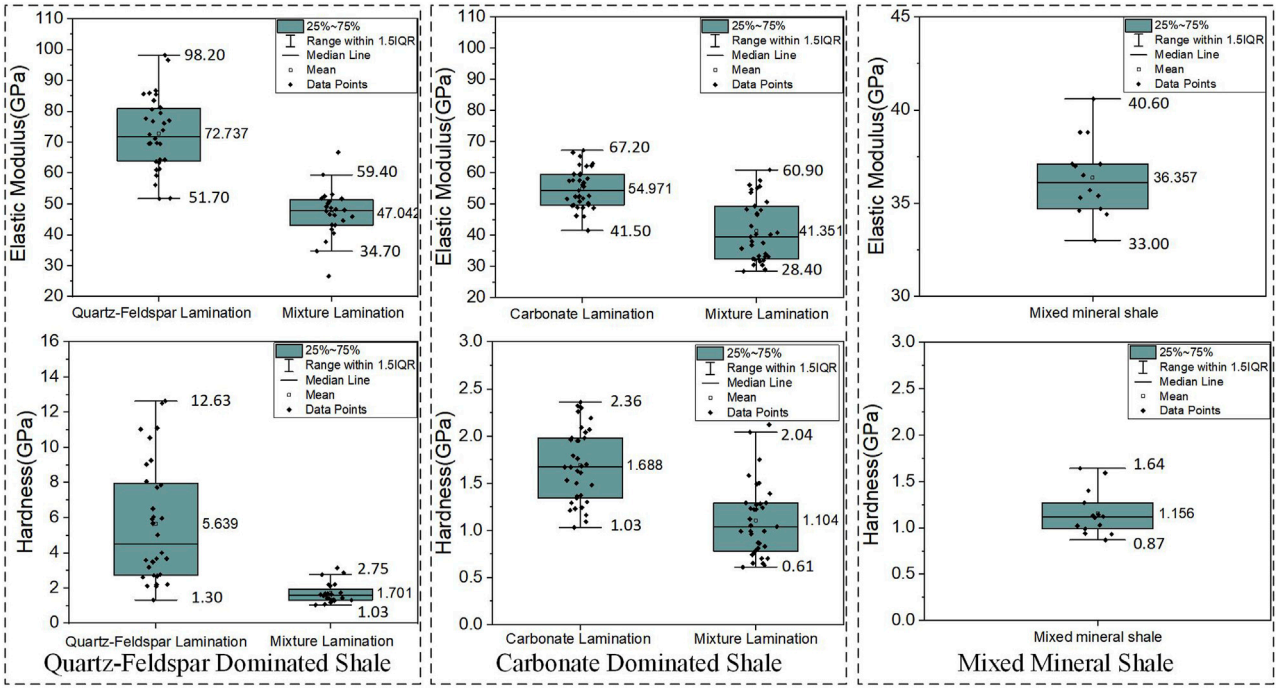

FIGURE 5
Micro indentation experiment results.

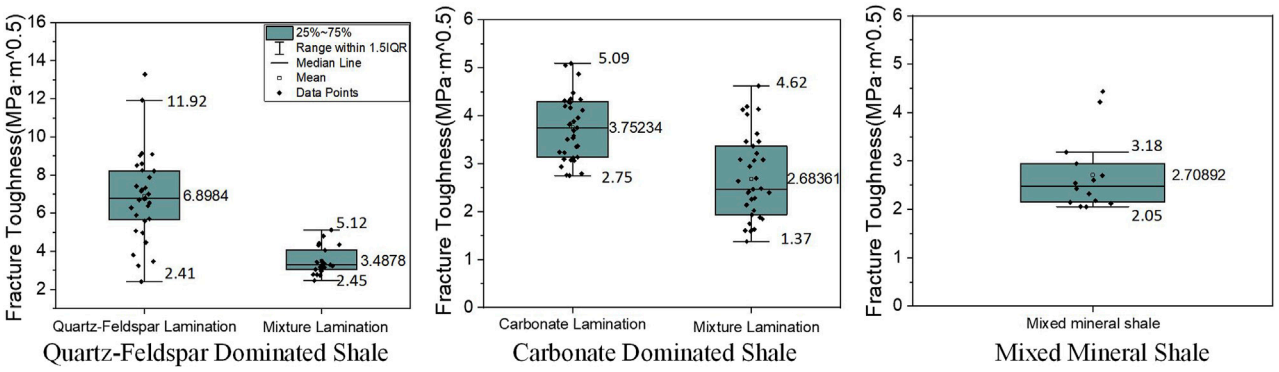

FIGURE 6
Fracture toughness of different laminations according to the Load-Displacement curves.

emission usually produces a large number of counts after sample failure because the sample continues to be compacted and cracked. The macroscopic cracks are mainly generated in the laminations and cracked along the lamination direction, as shown in Figure 7A. It can be observed that in these samples, the lamination is developed and the lamination thickness is small. Smaller lamination thickness exhibits lower total strength, resulting in more prone to cracking under stress. On the contrary, in Figure 7(a3), the lamination thickness is larger and the structure is more uniform. The mechanical test results show that its failure strength is high, the acoustic emission count is less and concentrated after the stress-strain peak, which confirms that fewer micro-cracks are generated during the loading process. Moreover, due to the multi-lamellar characteristics of the sample, the failure strength is relatively low, such as Sample No. (1, 2, 4, 5) in Figure 7A. Throughout the experiment, a substantial number of acoustic emission counts were recorded following the stress-strain peak, indicating that only a limited quantity of micro-cracks formed during the pre-peak loading stage. However, damage persisted after the peak as the weak surface of the lamination underwent progressive failure and compaction, ultimately resulting in complete sample failure. The lamination-developed samples eventually show the characteristics of macro fracture along the laminations.

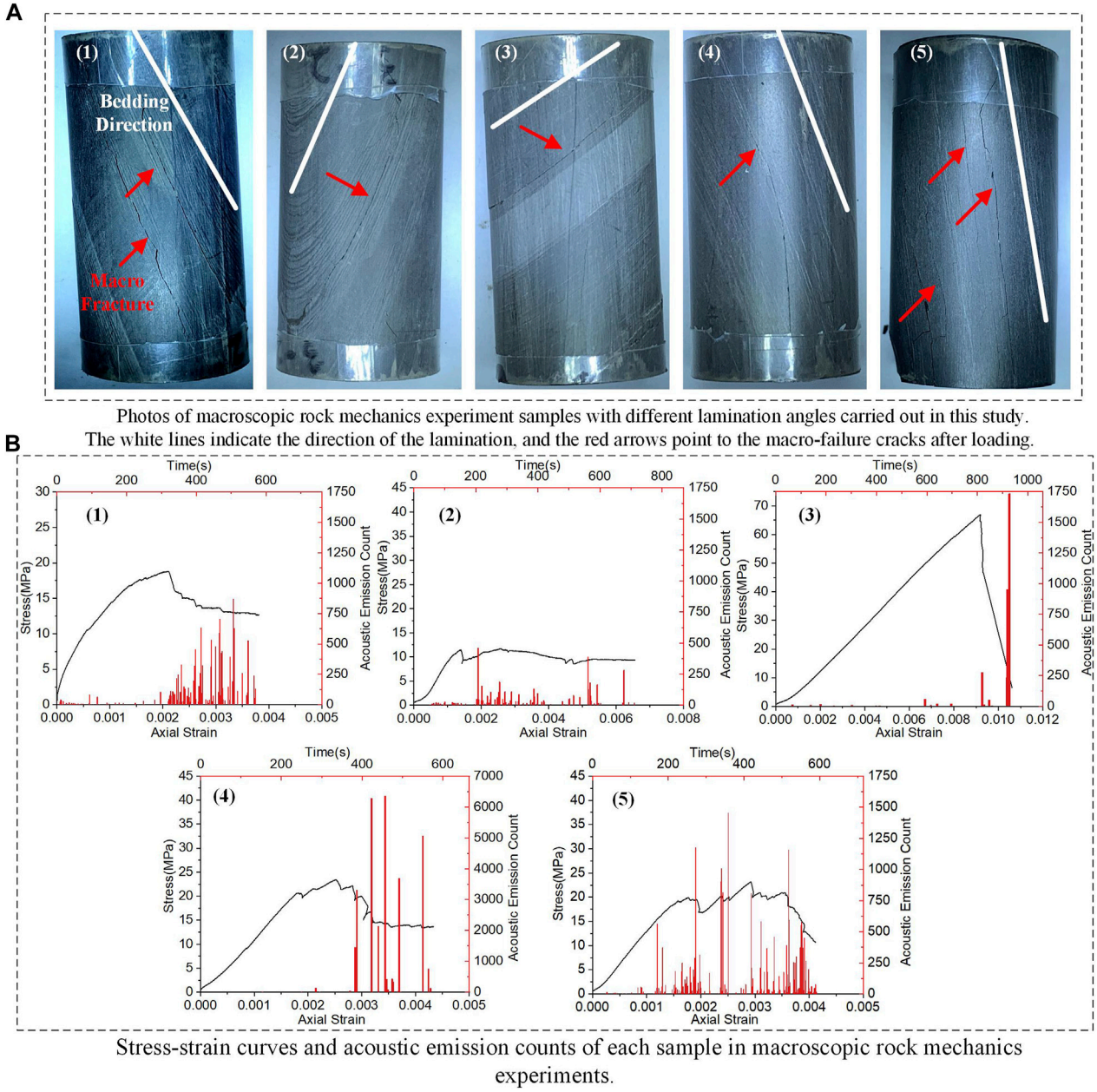

FIGURE 7
Macroscopic rock mechanics experiment results. **(A)** Photos of macroscopic rock mechanics experiment samples with different lamination angles carried out in this study. lie white lines indicate the direction of the lamination, and the red arrows point to the macro-failure cracks after loading. **(B)** Stress-strain curves and acoustic emission counts of each sample in macroscopic rock mechanics experiments.

4 Conclusion

Three laminations with different lithofacies of oil shale in the Third Member of Shahejie Formation in Qikou sag, Bohai Bay basin were identified through SEM and mineral analysis. The thickness of quartz-feldspar lamination commonly exceeds 400 μm on average because of its large grain size. The observed carbonate laminations are consistently smaller than 300 μm. The distinct laminations with different characteristics were precisely identified using FIB, which served as the navigation for the indentation experiment precisely. The micro mechanical properties of three distinct laminations were quantified using the nanoindentation method. This study investigates the mechanical differences between laminations in various lithofacies and reveals that Quartz-Feldspar dominated shales display significant variations in their mechanical characteristics, which ultimately promote the formation of fractures between different layers. Combined with macroscopic rock mechanics experiments, it is confirmed that distinct lithological lamination structure and micromechanical

variations of laminations in shale were microphysical and mechanical foundation for determining the initiation and propagation of macroscopic fractures. The micromechanical test results will be utilized in the subsequent step to establish a macroscopic mechanical model, aiming to investigate the correlation between lamination micromechanics and macroscopic rock mechanics.

Data availability statement

The raw data supporting the conclusions of this article will be made available by the authors, without undue reservation.

Author contributions

SC: Conceptualization, Data curation, Formal Analysis, Investigation, Methodology, Validation, Visualization, Writing–original draft. MS: Conceptualization, Data curation, Funding acquisition, Project administration, Validation, Writing–review and editing. CD: Formal Analysis, Investigation, Visualization, Writing–original draft.

Funding

The author(s) declare financial support was received for the research, authorship, and/or publication of this article. This research was funded by National Natural Science Foundation of China, grant number 52074315.

Conflict of interest

The authors declare that the research was conducted in the absence of any commercial or financial relationships that could be construed as a potential conflict of interest.

Publisher's note

All claims expressed in this article are solely those of the authors and do not necessarily represent those of their affiliated organizations, or those of the publisher, the editors and the reviewers. Any product that may be evaluated in this article, or claim that may be made by its manufacturer, is not guaranteed or endorsed by the publisher.

References

Chenevert, M. E., and Gatlin, C. (1965). Mechanical anisotropies of laminated sedimentary rocks. *Soc. Petroleum Eng. J.* 5, 67–77. doi:10.2118/890-PA

Cheng, S., Sheng, M., Chen, Z., Tian, S., and Li, G. (2021). "Identification of shale bedding layers from micromechanical evaluation," in Presented at SPE Annual Technical Conference and Exhibition 2021, ATCE 2021, Dubai, United arab emirates, September 21, 2021 - September 23, 2021, 2021 (Society of Petroleum Engineers SPE). doi:10.2118/206256-MS

Cheng, Y.-T., Li, Z., and Cheng, C.-M. (2002). Scaling relationships for indentation measurements. *Philos. Mag. A* 82, 1821–1829. doi:10.1080/01418610208235693

Huang, D., Li, B., Ma, W.-Z., Cen, D.-F., and Song, Y.-X. (2020). Effects of bedding planes on fracture behavior of sandstone under semi-circular bending test. *Theor. Appl. Fract. Mech.* 108, 102625. doi:10.1016/j.tafmec.2020.102625

Huang, L., Liu, J., Zhang, F., Dontsov, E., and Damjanac, B. (2019). Exploring the influence of rock inherent heterogeneity and grain size on hydraulic fracturing using discrete element modeling. *Int. J. Solids Struct.* 176-177, 207–220. doi:10.1016/j.ijsolstr.2019.06.018

Huang, L., Tan, J., Fu, H., Liu, J., Chen, X., Liao, X., et al. (2023). The non-plane initiation and propagation mechanism of multiple hydraulic fractures in tight reservoirs considering stress shadow effects. *Eng. Fract. Mech.* 292, 109570. doi:10.1016/j.engfracmech.2023.109570

Jin, Z., Li, W., Jin, C., Hambleton, J., and Cusatis, G. (2018). Anisotropic elastic, strength, and fracture properties of marcellus shale. *Int. J. Rock Mech. Min. Sci.* 109, 124–137. doi:10.1016/j.ijrmms.2018.06.009

Lei, B., Zuo, J., Liu, H., Wang, J., Xu, F., and Li, H. (2021). Experimental and numerical investigation on shale fracture behavior with different bedding properties. *Eng. Fract. Mech.* 247, 107639. doi:10.1016/j.engfracmech.2021.107639

Li, C., Ostadhassan, M., Kong, L., and Bubach, B. (2019). Multi-scale assessment of mechanical properties of organic-rich shales: a coupled nanoindentation, deconvolution analysis, and homogenization method. *J. Petroleum Sci. Eng.* 174, 80–91. doi:10.1016/j.petrol.2018.10.106

Li, W., Rezakhani, R., Jin, C., Zhou, X., and Cusatis, G. (2017). A multiscale framework for the simulation of the anisotropic mechanical behavior of shale. *Int. J. Numer. Anal. Methods Geomechanics* 41, 1494–1522. doi:10.1002/nag.2684

Liu, J., Liang, X., Xue, Y., Fu, Y., Yao, K., and Dou, F. (2020). Investigation on crack initiation and propagation in hydraulic fracturing of bedded shale by hybrid phase-field modeling. *Theor. Appl. Fract. Mech.* 108, 102651. doi:10.1016/j.tafmec.2020.102651

Liu, K., Ostadhassan, M., and Bubach, B. (2016). Applications of nano-indentation methods to estimate nanoscale mechanical properties of shale reservoir rocks. *J. Nat. Gas Sci. Eng.* 35, 1310–1319. doi:10.1016/j.jngse.2016.09.068

Maowen, L., Ma, X., Jin, Z., Li, Z., Jiang, Q., Wu, S., et al. (2022). Diversity in the lithofacies assemblages of marine and lacustrine shale strata and significance for unconventional petroleum exploration in China. *OIL GAS Geol.* 43, 1–25. doi:10.11743/ogg20220101

Mokhtari, M., Bui, B. T., and Tutuncu, A. N. (2014). "Tensile failure of shales: impacts of layering and natural fractures," in *Presented at SPE western north American and rocky mountain joint meeting*. SPE-169520-MS: All Days. doi:10.2118/169520-ms

Niandou, H., Shao, J. F., Henry, J. P., and Fourmaintraux, D. (1997). Laboratory investigation of the mechanical behaviour of tournemire shale. *Int. J. Rock Mech. Min. Sci.* 34, 3–16. doi:10.1016/S1365-1609(97)80029-9

Oliver, W., and Pharr, G. (1992). An improved technique for determining hardness and elastic modulus using load and displacement sensing indentation experiments. *J. Mater. Res.* 7, 1564–1583. doi:10.1557/JMR.1992.1564

Phani, P. S., Oliver, W. C., and Pharr, G. M. (2020). Understanding and modeling plasticity error during nanoindentation with continuous stiffness measurement. *Mater. Des.* 194, 108923. doi:10.1016/j.matdes.2020.108923

Sayers, C. M. (2013). The effect of anisotropy on the young's moduli and Poisson's ratios of shales. *Geophys. Prospect.* 61, 416–426. doi:10.1111/j.1365-2478.2012.01130.x

Sheng, M., Cheng, S.-Z., Lu, Z.-H., Zhang, Y., Tian, S.-C., and Li, G.-S. (2022). Influence of formation in-situ stress on mechanical heterogeneity of shale through grid nanoindentation. *Petroleum Sci.* 19, 211–219. doi:10.1016/j.petsci.2021.10.006

Shi, Z., Dong, D., Wang, H., Sun, S., and Wu, J. (2020). Reservoir characteristics and genetic mechanisms of gas-bearing shales with different laminae and laminae combinations: a case study of member 1 of the lower silurian longmaxi shale in sichuan basin, sw China. *PETROLEUM Explor. Dev.* 47, 888–900. doi:10.1016/s1876-3804(20)60104-5

Tan, P., Chen, Z., Fu, S., and Zhao, Q. (2023). Experimental investigation on fracture growth for integrated hydraulic fracturing in multiple gas bearing formations. *Geoenergy Sci. Eng.* 231, 212316. doi:10.1016/j.geoen.2023.212316

Tan, P., Jin, Y., Han, K., Hou, B., Chen, M., Guo, X., et al. (2017). Analysis of hydraulic fracture initiation and vertical propagation behavior in laminated shale formation. *Fuel* 206, 482–493. doi:10.1016/j.fuel.2017.05.033

Tan, P., Jin, Y., and Pang, H. (2021). Hydraulic fracture vertical propagation behavior in transversely isotropic layered shale formation with transition zone using xfem-based czm method. *Eng. Fract. Mech.* 248, 107707. doi:10.1016/j.engfracmech.2021.107707

Ulm, F.-J., and Abousleiman, Y. (2006). The nanogranular nature of shale. *Acta Geotech.* 1, 77–88. doi:10.1007/s11440-006-0009-5

Ulm, F.-J., Vandamme, M., Bobko, C., Alberto Ortega, J., Tai, K., and Ortiz, C. (2007). Statistical indentation techniques for hydrated nanocomposites: concrete, bone, and shale. *J. Am. Ceram. Soc.* 90, 2677–2692. doi:10.1111/j.1551-2916.2007.02012.x

Vernik, L., and Nur, A. (1992). Ultrasonic velocity and anisotropy of hydrocarbon source rocks. *Geophysics* 57, 727–735. doi:10.1190/1.1443286

Xiugang, P., Miaochao, M., Bincheng, G., Kejia, Z., Congsheng, B., Jianying, M., et al. (2023). Shale lithofacies characteristics and shale oil bearing differences in the es3^{s} of qibei subsag, oikou sag, bohai bay basin. *J. Northeast Petroleum Univ.* 47, 55–69. doi:10.3969/.issn.2095-4107.2023,02.005

Yang, L., Sharafisafa, M., and Shen, L. (2021). On the fracture mechanism of rock-like materials with interbedded hard-soft layers under brazilian tests. *Theor. Appl. Fract. Mech.* 116, 103102. doi:10.1016/j.tafmec.2021.103102

Zeng, Q., Feng, Y., and Xu, S. (2017). A discussion of "application of nano-indentation methods to estimate nanoscale mechanical properties of shale reservoir rocks" by k liu, m osatadhassan and b bubach. *J. Nat. Gas Sci. Eng.* 42, 187–189. doi:10.1016/j.jngse.2017.02.027

Zhang, Y., Liu, Z., Han, B., Zhu, S., and Zhang, X. (2022). Numerical study of hydraulic fracture propagation in inherently laminated rocks accounting for bedding plane properties. *J. Petroleum Sci. Eng.* 210, 109798. doi:10.1016/j.petrol.2021.109798

Zhijun, J., Rukai, Z., Xinping, L., and Yunqi, S. (2021). Several issues worthy of attention in current lacustrine shale oil exploration and development. *PETROLEUM Explor. Dev.* 48, 1276–1286. doi:10.11698/PED.2021.06.20

Zhu, Y., Liu, K., Zhong, X., Wang, Y., Chen, C., Zhang, H., et al. (2021). Experimental investigation on the anisotropic behaviors induced by bedding planes in mechanical properties of ma′quan oil shale. *Arabian J. Sci. Eng.* 47, 11385–11403. doi:10.1007/s13369-021-06027-2